Semiclassical evaluation of nonadiabatic rates in condensed phases

Eyal Neria and Abraham Nitzan
School of Chemistry, the Sackler Faculty of Science, Tel Aviv University, Tel Aviv, 69978, Israel

(Received 20 October 1992; accepted 19 March 1993)

A procedure for calculating nonadiabatic transition rates in the semiclassical limit is implemented and tested for models relevant for condensed phase processes. The method is based on evaluating the golden rule rate expression using a quantum description for the electronic subsystem and a semiclassical propagation for the nuclear degrees of freedom, similar to Heller's calculation of absorption and Raman spectra. In condensed phase processes, the short lifetimes of the relevant correlation functions make it possible to implement the procedure within the frozen Gaussian method. Furthermore, because of the large density of states involved, which implies fast dephasing, incoherent superpositions of frozen Gaussian trajectories may be used for the evaluation of the rate. The method is tested using two simple exactly soluble models. One of them, consisting of two coupled electronic potential surfaces, harmonic and linear, is also used for testing and comparing a recently proposed algorithm by Tully. The other, the well-known displaced harmonic potentials model, is a prototype of many condensed phase processes. Finally, the method is applied for calculating the nonadiabatic radiationless relaxation of the solvated electron from its first excited state to the fully solvated ground state.

I. INTRODUCTION

There has been much activity in the past few years aimed at developing methods for simulation of quantum processes in condensed phases.[1,2] Because of restrictions imposed by available computing resources, most approaches use some form of mixed quantum-classical representation of the system. The idea behind this approach is that, for many processes in condensed phases, quantum mechanics may govern only the time evolution of solute molecules under study, whereas the motion of the surrounding thermal bath is essentially classical. This is the basis for several calculations which apply a variety of methods for mixed quantum classical calculations, e.g., path integral Monte Carlo,[1(b),1(c)] path integral molecular dynamics,[1(c),1(d)] the Car–Parrinello density functional approach,[1(e)] and the quantum-classical time dependent self-consistent field (TDSCF) approximation.[1(f),1(g)] Of these, only the latter is capable of treating excited states and quantum dynamical phenomena.

In mixed quantum-classical approximations of the SCF type (including the path integral and the Car–Parrinello method), the force exerted on the classical particles by the quantum subsystem is approximated by the corresponding expectation value with the instantaneous wave function of the latter. This is a reasonable approximation when the quantum subsystem explores the probability space occupied by its wave function on a time scale short compared with the characteristic time of the classical system. When this is not so, e.g., when the quantum motion involves slow tunneling between two distinct subspaces, SCF approximations may fail badly.[1(g),3,4] It is important to realize that this is a failure of the SCF scheme, not of the mixed quantum classical representation *per se*. A fully quantum Hartree approximation will also fail under similar circumstances. In such cases, multiconfiguration TDSCF[1(g),3,4] provides a practical generalization, similar to configuration interaction methods in time independent calculations. In this approach, the wave function for the total system is represented as a sum of Hartree-like products $\Psi(s,b,t)=\Sigma_i\phi_i(s,t)\kappa_i(b,t)$, where s and b denote "system" and "bath" coordinates, respectively. However, unlike its single configuration counterpart, the MC-TDSCF cannot be carried over to the mixed quantum-classical representation in which the time evolution of $\kappa(b,t)$ is replaced by classical equations of motion.

A special case in which the quantum subspace is strongly divided and simple SCF fails is when the process under study involves nonadiabatic transitions between different states of the quantum subsystem. Here the classical subsystem is associated with different potential surfaces for the different quantum states, and applying the simple TDSCF scheme amounts to replacing these by a mean potential whose value is determined by the instantaneous populations of the different quantum states. Again this may fail very badly as has been discussed by several authors.[1(g),4–7] A practical quantum-classical approximation for this class of problems is provided by the Tully–Preston surface hopping technique,[8] in which classical motion is carried on isolated potential surfaces, except at near crossing locations, where Landau–Zener[9] or an equivalent theory is used to assign new populations to the different quantum states. Obviously this method is limited to processes in which the nonadiabatic transitions are dominated by surface crossing events. An important generalization of this approach was recently provided by Webster *et al.*[10] and applied to describing solvation of an excess electron in water. In this approach, the force on the classical subsystem is calculated, during a short coherence time Δt, using the Pechukas theory[11] which provides an expression for the effective force on the classical subsystem in terms of the full quantum path taken by the quantum subsystem. Because of the self-consistent iterative manner in which this effective force has to be calculated, this method is highly

CPU demanding and can be applied reliably mainly to cases where the transition is dominated by isolated surface crossing events. Also, the dependence of this method on the choice of the coherence time Δt is a drawback that will need further studies in future applications.

Another generalization of the surface hopping technique was recently suggested by Tully.[5] In this algorithm, as in the original surface hopping method, trajectories evolve on individual surfaces and make instantaneous hops from one state to another with corresponding velocity adjustment to conserve energy, however, hops can occur anywhere in space and time as governed by quantum transition probabilities, provided energy can be conserved. The algorithm is supplemented by the "fewest switches criterion" designed to achieve the correct fraction of classical trajectories assigned to each quantum state with the minimum number of state switches. It was recently applied to the dynamics of electron solvation in liquid helium by Space and Coker.[12]

The important advantage of the new Tully method[5] over the original surface hopping approach[8] is that it can be applied to transitions which are not dominated by distinct surface crossing events. Many such situations are characterized by weak coupling between the quantum states involved, and consequently, the transitions are slow so that evaluating rates can become very costly. Also this algorithm cannot be applied to tunneling transitions (e.g., the Landau–Zener curve crossing model with initial energy below the surface crossing energy) because of the inherent classical nature of the trajectory. On the other hand, in most such situations, perturbation theory is valid. This suggests that a direct evaluation of the perturbation theory expression for the transition rate using some form of mixed quantum-classical simulations may be a useful alternative route for studying many nonadiabatic processes.

To be specific, consider the golden rule expression for the thermal transition rate between two electronic states 1 and 2

$$k_{1\to 2}=\frac{2\pi}{\hbar}\sum_i \frac{e^{-\beta E_{1i}}}{Z_1}\sum_f |\langle 1i|V|2f\rangle|^2\delta(E_{1i}-E_{2f}), \tag{1}$$

where $\beta=(k_BT)^{-1}$ and $Z_1=\Sigma e^{-\beta E_{1i}}$. $|i\rangle$ and $|f\rangle$ are nuclear states associated with the initial $|1\rangle$ and the final $|2\rangle$ electronic states, respectively. Denoting $V_{12}=\langle 1|V|2\rangle$ (still an operator in the nuclear subspace), Eq. (1) may be rewritten as a Fourier transform of a correlation function

$$k_{1\to 2}=\int_{-\infty}^{\infty} dt\, e^{i\Delta Et/\hbar}C(t), \tag{2}$$

where ΔE is the difference between the energy origin of surface 2 and 1

$$C(t)=Z^{-1}\hbar^{-2}\sum_i e^{-\beta E_i}\langle i|V_{12}e^{iH_2t/\hbar}V_{21}e^{-iH_1t/\hbar}|i\rangle$$
$$\equiv\hbar^{-2}\langle V_{12}e^{iH_2t/\hbar}V_{21}e^{-iH_1t/\hbar}\rangle_T. \tag{3}$$

In Eq. (3), H_1 and H_2 are the nuclear Hamiltonians associated with the electronic states $|1\rangle$ and $|2\rangle$, respectively, each measured from its own electronic origins. This suggests that the rate may be obtained from a classical or semiclassical evaluation of the correlation function $C(t)$. Heller[13] has used this approach in his evaluation of optical and Raman line shapes using Gaussian wave packets. More recently, the same approach was used by Herman[14] for vibrational relaxation and by Villareal *et al.*[15] for vibrational predissociation. A different method was recently used by Haug and Metiu[16] for absorption spectra in a mixed quantum classical system by using a swarm of trajectories to represent a "classical" wave function for the essentially classical coordinate.

In a recent preliminary report,[17] we have used this approach to calculate the rate of the nonadiabatic radiationless transition from the first excited state of the hydrated electron to the ground fully solvated state of this species. This calculation has followed recent reports[18,19] which indicated that the observed evolution of absorption spectra associated with electrons injected into liquid water cannot be accounted for by an adiabatic evolution on a single potential surface. We have used the golden rule approach described above, where the correlation function $C(t)$ was evaluated using classical molecular dynamics for the water molecules in the two electronic states. There were two new elements in this calculation: (a) because the adiabatic potential surfaces associated with the ground and excited states of the hydrated electron are not known, they were evaluated in the course of the simulation by evaluating the electronic energies, the forces on the nuclei, and the coupling matrix elements V_{12} at every nuclear position. (b) Classical mechanics for the nuclei is not sufficient for this calculation because of the expected role of Franck–Condon factors in determining the values of the matrix elements $\langle 1i|V|2f\rangle$, so semiclassical wave packets were used as in Refs. 13 and 15. However, we have argued that because of the short lifetime of $C(t)$ in condensed phase processes [$C(t)$ was shown to decay to zero with a lifetime of $\sim$10 fs], frozen Gaussians[20] were sufficient for this calculation. Consequently, with a proper choice of the Gaussians widths, all the needed information is obtained from classical nuclear trajectories.

The present article has three objectives: (a) we critically examine the use of frozen Gaussian wave packets for evaluating golden rule rates of the form (1) by comparing results for simple models for which the golden rule can be calculated exactly; (b) we test the performance of the Tully algorithm for one of these models for which the exact time evolution may also be calculated; (c) we provide details and corrected results for the application of the golden rule approach to the nonadiabatic hydration dynamics of an injected electron.

The method is reviewed in Sec. II. Application to the (exactly soluble) model, which involves one harmonic and one linear one dimensional potential surfaces, is described in Sec. III, where a comparison to the performance of the Tully method is also presented. In Sec. IV, we discuss the performance of the frozen Gaussian-golden rule method

within the displaced harmonic potentials model, for which the golden rule rate can be evaluated exactly. Finally, in Sec. V, we describe the application of this approach to the nonadiabatic solvation dynamics of an electron. We conclude in Sec. VI.

II. THE METHOD

The golden rule expressions (1)–(3) are a result of perturbation theory and, within the limits of its validity, can be used with many choices of zero order states and perturbations as dictated by the nature of the particular problems. In the simple models discussed in Secs. III and IV, we consider diabatic potential surfaces coupled by a constant (i.e., independent of nuclear position) perturbation. For these cases, the correlation function $C(t)$ [Eq. (3)] takes the form

$$C(t)=\frac{|V_{12}|^2}{\hbar^2}\langle e^{iH_2t/\hbar}e^{-iH_1t/\hbar}\rangle_T, \tag{4}$$

where the thermal average is taken over the distribution of nuclear states on the initial potential surface. In actual application, e.g., the calculation described in Sec. V of the radiationless transition from an excited to the ground state of a solvated electron, the initial and final electronic states are assumed to be the Born–Oppenheimer adiabatic states and the perturbation V is the nonadiabatic coupling resulting from the nuclear kinetic energy. In this case, the coupling depends on both nuclear positions and momenta. In what follows, we describe the calculation in terms of this coupling. The matrix element $\langle 1i|V|2f\rangle$ is approximated by

$$\langle 1i|V|2f\rangle=\sum_l (M_l)^{-1}\langle\chi_i^{(1)}|\hat{\mathbf{P}}_l\langle\phi_1|\hat{\mathbf{P}}_l|\phi_2\rangle|\chi_f^{(2)}\rangle \tag{5}$$

where ϕ_1 and ϕ_2 are eigenstates of the electronic Hamiltonian $H_e=T_e+V_{ee}+V_{eN}+V_{NN}$ (containing the electrons' kinetic energy T_e, the electron–electron interaction V_{ee}, the electron–nuclear interaction V_{eN}, and the nuclear–nuclear interaction V_{NN}, respectively) and where $\chi_i^{(1)}$ and $\chi_f^{(2)}$ are eigenstates of the nuclear Hamiltonian $H_1=T_N+\langle\phi_1|H_e|\phi_1\rangle$ and $H_2=T_N+\langle\phi_2|H_e|\phi_2\rangle$. $T_N=\Sigma_l P_l^2/2M_l$ (the sum is over nuclei) is the nuclear kinetic energy expressed in terms of the nuclear masses M_l and nuclear momenta P_l. Note that in Eq. (5), we have disregarded terms containing a second derivative of the electronic wave functions with respect to the nuclear coordinates (see below). Using Eq. (5), the rate $k_{1\to2}$ and the correlation function $C(t)$ takes the form

$$k_{1\to2}=\int_{-\infty}^{\infty}dt\,C(t), \tag{6a}$$

$$C(t)=\sum_{ll'}(M_lM_{l'}Z_1)^{-1}\sum_i e^{-\beta E_{1i}}\times\langle\chi_i^{(1)}|\mathbf{F}_l\cdot\hat{\mathbf{P}}_l e^{iH_2t/\hbar}\hat{\mathbf{F}}_{l'}\cdot\hat{\mathbf{P}}_{l'}e^{-iH_1t/\hbar}|\chi_i^{(1)}\rangle, \tag{6b}$$

where $\hat{\mathbf{F}}_l=\hbar^{-1}\langle\phi_1|\hat{\mathbf{P}}_l|\phi_2\rangle$. The function $\hat{\mathbf{F}}_l$ is also equal to the matrix element of the force between the two adiabatic states

$$\hat{\mathbf{F}}_l=i\frac{\langle\phi_1|\partial V_{eN}/\partial\mathbf{R}_l|\phi_2\rangle}{E_1-E_2}. \tag{7}$$

Note that in contrast to Eqs. (2) and (3), the Hamiltonians H_1 and H_2 in Eq. (6b) are measured from a common energy origin. Therefore, the term $\exp(i\Delta Et)$ which appears explicitly in Eq. (2) is now contained in Eq. (6b).

Our semiclassical calculation of the correlation function (6b) is based on the observation that close to the classical limit it can be approximated by

$$C(t)=\left\langle\sum_l\sum_{l'}\mathbf{F}_{l'}[\mathbf{R}^{(2)}(t)]\cdot\mathbf{v}_{l'}^{(2)}(t)\mathbf{F}_l[\mathbf{R}^{(1)}(0)]\mathbf{v}_l^{(1)}\times(0)J(t)\right\rangle_T, \tag{8a}$$

$$J(t)=\langle G^{(2)}[\mathbf{R}^{(2)}(t),\mathbf{P}^{(2)}(t)]|G^{(1)}[\mathbf{R}^{(1)}(t),\mathbf{P}^{(1)}(t)]\rangle \tag{8b}$$

where $\mathbf{v}=\mathbf{P}/m$ and $\langle\ \rangle_T$ denotes thermal averaging. $\mathbf{R}^{(\alpha)}(t)$ and $\mathbf{v}^{(\alpha)}(t)$ ($\alpha=1,2$) are classical positions and velocities evaluated on the electronic surface α starting with initial conditions $\mathbf{R}^{(1)}(0),\mathbf{v}_1^{(1)}(0)$. These initial conditions are sampled from the canonical distribution on surface 1 to achieve thermal averaging. The function $|G^{(\alpha)}[\mathbf{R}^{(\alpha)}(t),\mathbf{P}^{(\alpha)}(t)]\rangle$ is a product, over the classical atoms, of frozen Gaussians whose time evolution follows the classical trajectory

$$\langle\mathbf{R}|G^{(\alpha)}[\mathbf{R}^{(\alpha)}(t),\mathbf{P}^{(\alpha)}(t)]\rangle=\prod_l G_l^{(\alpha)}(\mathbf{R}_l,t)\exp\left[i/\hbar\int_0^t L^{(\alpha)}(t')dt'\right], \tag{9a}$$

$$G_l^{(\alpha)}(\mathbf{R}_l,t)=G[\mathbf{R}_l|\mathbf{R}_l^{(\alpha)}(t),\mathbf{P}_l^{(\alpha)}(t)]\equiv(a_l/\pi)^{3/4}\exp\left\{-\frac{1}{2}a_l\left|\mathbf{R}_l-\mathbf{R}_l^{(\alpha)}(t)\right|^2+i/\hbar\mathbf{P}_l^{(\alpha)}(t)\cdot[\mathbf{R}_l-\mathbf{R}_l^{(\alpha)}(t)]\right\}, \tag{9b}$$

$$L^{(\alpha)}=\sum_l[\mathbf{P}_l^{(\alpha)}(t)]^2/M_l-\left\langle\prod_l G_l^{(\alpha)}\left|H_\alpha\right|\prod_l G_l^{(\alpha)}\right\rangle. \tag{9c}$$

Once we limit ourselves to frozen Gaussians, the time evolution needed to evaluate $J(t)$ and $C(t)$ is purely classical. It is important to note, however, that since the trajectories needed to evaluate $J(t)$ [Eq. (8b)] evolve on different potential surfaces, the quantum mechanical phases associated with the Lagrangian (9c) do not cancel and may contribute in a significant way to the final result. Note also that the initial conditions for the time evolutions are identical for the two potential surfaces. In order to evaluate $C(t)$ [Eq. (8a)], these initial conditions are sampled from an approximate thermal distribution associated with the initial nuclear Hamiltonian H_1. In the present application, we approximate this thermal averaging by

sampling from a classical canonical distribution on surface 1. This high temperature approximation can be improved upon in several ways that will be described in a subsequent paper.

Finally, note that even though the two trajectories used to evaluate $J(t)$ start from the same positions and momenta, the corresponding energies are different since they evolve on different surfaces. This nonenergy conserving nature of the trajectories which stand in marked contrast to the usual surface hopping methods is not a matter of concern here because we do not evaluate the physical time evolution of the systems, but only information needed to calculate the transition rate.

In Sec. III, we also examine the use of frozen Gaussians to calculate the transition rate out of a particular nuclear quantum state $\chi_n^{(1)}(R)$ (with energy E_{1n}) of H_1. This can be done on two levels:

(a) Following Heller,[20,21] the initial state is represented as a superposition of N Gaussians, characterized by some chosen width to be discussed below, distributed evenly on the energy shell $E(\mathbf{P},\mathbf{R})=E_{1n}$,

$$\chi(\mathbf{R})=\sum_{j=1}^{N} C_j G_j(\mathbf{R}) \quad [E(\mathbf{P}_j,\mathbf{R}_j)=E_{1n}]. \tag{10a}$$

The correlation function $C(t) = \langle\chi| V_{12} e^{iH_2 t/\hbar} V_{21} \times e^{-iH_1 t/\hbar}|\chi\rangle$ then becomes

$$C(t)=\sum_j \sum_k C_j^* C_k \langle G_j| V_{12} e^{iH_2 t/\hbar} V_{12} e^{-iH_1 t/\hbar}|G_k\rangle. \tag{10b}$$

The matrix element in Eq. (10b) is then evaluated in the frozen Gaussians approximation (FGA) as described above. In this case, the time evolved Gaussians are added coherently to form $C(t)$.

(b) The initial position and momenta are sampled from a classical microcanonical distribution characterized by the energy E_{1n} (a better approximation, e.g., using a Wigner distribution, can be used). A proper width is chosen for the Gaussians centered about this initial position and momenta. The correlation function is calculated for this Gaussian by evolving it on the two surfaces, and finally an ensemble averaged over the initial position and momenta is formed. This amounts to neglecting the nondiagonal terms in Eq. (10b) and to take all $|C_j|^2$ the same (i.e., $1/N$) for all initial samples which correspond to the given initial energy. While the latter scheme involving incoherent superposition of Gaussians is obviously inferior to the former, this is a useful approximation for microcanonical rates in condensed phase systems where the potential surfaces (hence the initial nuclear wave function) are not known. In such systems, many initial quantum states contribute within the experimental energy resolution, and coherencies associated with the nondiagonal terms in Eq. (10b) are expected to wash out.

In many applications, e.g., Sec. V, the potential surfaces $E_\alpha(\mathbf{R})$ are not known, but can be evaluated *locally* in mixed electronic (quantum)–nuclear (classical) simulations. In such simulations, the relevant electronic wave functions $\phi_\alpha(\mathbf{R})$ and energies $E_\alpha(\mathbf{R})$ are obtained for the instantaneous nuclear position R, and the nuclei move classically under the combined influence of their mutual interactions and the expectation value of their interaction with the electron(s) $\langle\phi_1|\partial V_{eN}/\partial R|\phi_1\rangle$ evaluated with the electronic wave function $\phi_1(\mathbf{R})$ of the initial electronic state. It is important to note that in this calculation of the electronic transition rate, the needed electronic interaction is only that contained in the adiabatic wave functions and energies. The nonadiabatic coupling is obtained as a function of nuclear position using Eq. (7). We note in passing that another nonadiabatic coupling term $\langle\phi_1|P_l^2|\phi_2\rangle$ that was disregarded in Eq. (6) can be evaluated in a similar way using the relation

$$\left\langle \phi_1 \left| \frac{\partial^2}{\partial R_l^2} \right| \phi_2 \right\rangle = -\frac{\langle\phi_1|\partial^2 V_{eN}/\partial R_l^2|\phi_2\rangle}{E_1-E_2} + \sum_{n\neq 2} \frac{\langle\phi_1|\partial V_{eN}/\partial \mathbf{R}_l|\phi_n\rangle\langle\phi_n|\partial V_{eN}/\partial \mathbf{R}_l|\phi_2\rangle}{(E_1-E_n)(E_n-E_2)}.$$

Obviously, the sum in the second term has to be truncated.

Such adiabatic simulations have been used recently[22–25] to calculate spectroscopic and transport phenomena associated with the solvated electron. A preliminary report of our application to nonadiabatic solvation of an electron in water has been recently published.[17] We note that adiabatic simulations using the Car–Parrinello[1(e)] method cannot be used at present for such applications because it is not suitable for calculating excited electronic states.

The procedure described above is only one of several possible approximation schemes. In particular, the use of the frozen Gaussians approximation (FGA) could be avoided; the variational Heller propagation method[26] could be employed with a modest increase in computational effort. However, FGA is expected to be valid for most condensed phase processes because of the fast decay of the correlation function $C(t)$. The reason for this is that during the short lifetime of $C(t)$, the classical motion spans only very limited space and the atoms do not move far enough to explore the anharmonicity of their local environment.

Another approximation employed in Eqs. (8) and (9) is the separability of G as a product over atomic Gaussian functions. Again this approximation is expected to do well for short times. A better but costlier alternative is to express G as a product of Gaussians defined for the normal modes associated with the local harmonic approximation to $E_\alpha(\mathbf{R})$.

Finally, we discuss the choice of the frozen widths $a_l^{-1/2}$ of the Gaussians in Eq. (9b). For the coherent expansion of individual energy levels [Eq. (10b)] of the harmonic oscillator in Sec. III, we have used the standard coherent states of the harmonic oscillator which are Gaussians whose width is that of the ground state wave function $\{a=[(m\omega)/\hbar]^{1/2}\}$. For high temperatures, the width is chosen to minimize the error resulting from the application

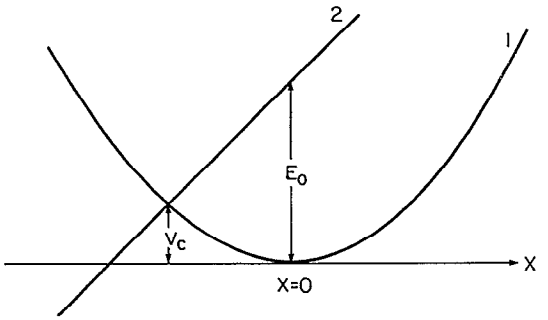

FIG. 1. A scheme of the potential surfaces used for modeling transitions between a harmonic and a linear surface.

of this method to the thermal transition rate in the displaced harmonic oscillators model. This leads to (see Sec. IV)

$$a=\frac{6mk_BT}{\hbar^2}\simeq\left(\frac{\lambda_{\rm th}}{6}\right)^{-2}. \tag{11}$$

As could be expected, $a^{-1/2}$ is of the order of the thermal de Broglie wavelength $\lambda_{\rm th}$ and has the convenient property of being independent of the local potential surface. At lower temperatures, the choice of the Gaussian width is less straightforward. For a harmonic oscillator at $T=0$, the width of the ground state Gaussian is $[(m\omega)/\hbar]^{-1/2}$. This will be our choice also for anharmonic systems, provided that they can be represented for each nuclear configuration as a collection of stable normal modes using the local harmonic approximation. This issue will be considered in a future publication.

In what follows, we describe several application and critical tests of the methods described above.

III. TRANSITION BETWEEN HARMONIC AND LINEAR SURFACES

Here we apply the method to a simple model for which both the exact golden rule rate and the exact full time evolution may be calculated. We also use the same model to evaluate the time evolution according to the Tully molecular dynamics with electronic transitions (MDET) method.[5]

The model consists of two diabatic surfaces. An initial harmonic surface 1 coupled to a linear surface 2 with a constant interaction V_{12} (Fig. 1). We use dimensionless representation in which the coordinate, the momentum, and energy are given in units of $[\hbar/(m\omega)]^{1/2}$, $(m\hbar\omega)^{1/2}$, and $\hbar\omega$, respectively. The potential surfaces are given in these units by

$$V_1=\tfrac{1}{2}X^2, \tag{12a}$$

$$V_2=\alpha X+E_0; \tag{12b}$$

changing E_0 amounts to changing the crossing energy $V_C=\alpha\pm\sqrt{\alpha^2+2E_0}$ of the two surfaces. In all the calculations presented, we used $\alpha=6$ (the same parameter was used by Heller[13(a)] in a similar context).

In the diabatic representation, the correlation function $C(t)$ for the thermal rate is given by Eq. (4)

$$C(t)=\frac{V_{12}^2}{\hbar^2Z_1}\sum_i e^{-\beta E_{1i}}\langle\chi_i^{(1)}|e^{iH_2t/\hbar}e^{-iH_1t/\hbar}|\chi_i^{(1)}\rangle \tag{13}$$

and the semiclassical approximation is invoked by replacing Eq. (13) by

$$C(t)=\frac{V_{12}^2}{\hbar^2}\langle J(t)\rangle_T \tag{14}$$

with $J(t)$ given by Eq. (8b). We also consider transitions out of a single quantum state of the harmonic surface as discussed above.

Consider first the transition rate from a single energy level of the harmonic potential to the linear potential. The golden rule expression for this rate can be obtained exactly as outlined in Appendix A. Following the procedure described in Sec. II, we represent the initial harmonic wave function as a coherent superposition of Gaussians, and propagate these Gaussians according to the FGA. It is convenient to use for this expansion the standard harmonic oscillator coherent states,[20,21] which are Gaussians whose width is that of the ground state of the oscillator [i.e., $a=(m\omega)/\hbar$ in Eq. (9b)]. Taking the initial wave function to be the nth level of the harmonic surface, the expansion in terms of N such Gaussian wave functions takes the form

$$\chi_n(X)=\sum_{j=1}^{N}C_jG_j(X), \tag{15a}$$

$$C_j=\frac{\sqrt{n!}}{NE_n^{n/2}}\exp(E_n/2)\exp(in\tau_j+iP_jX_j/2), \tag{15b}$$

where $\tau_j=(2\pi/N)j$, $j=1,2,...,N$, $X_j=\sqrt{2E_n}\cos(\tau_j)$, $P_j=\sqrt{2E_n}\sin(\tau_j)$, and $E_n=n+1/2$. $G_j(X)$ are one dimensional Gaussians [Eq. 9(b)] with averaged position X_j and momentum P_j.

The comparison between the exact and the "coherent" FGA calculations [based on Eq. (10b)] of the transition rate from the $n=11$ level of the harmonic oscillator is shown in Fig. 2(a) as a function of E_0. The number of Gaussians used in this calculation is $N=300$. For $E_0=40.3$, the surfaces cross at the energy of the 11th oscillator level $V_c=E_{n=11}=(n+1/2)$. For $E_0>40.3$, the initial energy $E_{n=11}$ is smaller than the crossing energy and the transition takes place by tunneling. We see that the agreement is very good even at the tunneling regime as long as the rate is not too small. The observed oscillations result from the structure of the initial harmonic ($n=11$) wave function which has 12 maxima. For values of E_0 for which the peak in the Airy function [the eigenfunction of the linear potential (see Appendix A)] overlaps a peak in the harmonic wave function, the golden rule rate goes through a maximum as seen in the figure. Figure 2(a) also shows the result of the corresponding incoherent approximation using the same number $N=300$ of Gaussians and keeping only the diagonal terms $j=k$ in Eq. (10b). Note that while the Gaussians used in the coherent expansion are the coherent states whose dimensionless width is $a^{-1/2}=[\hbar/$

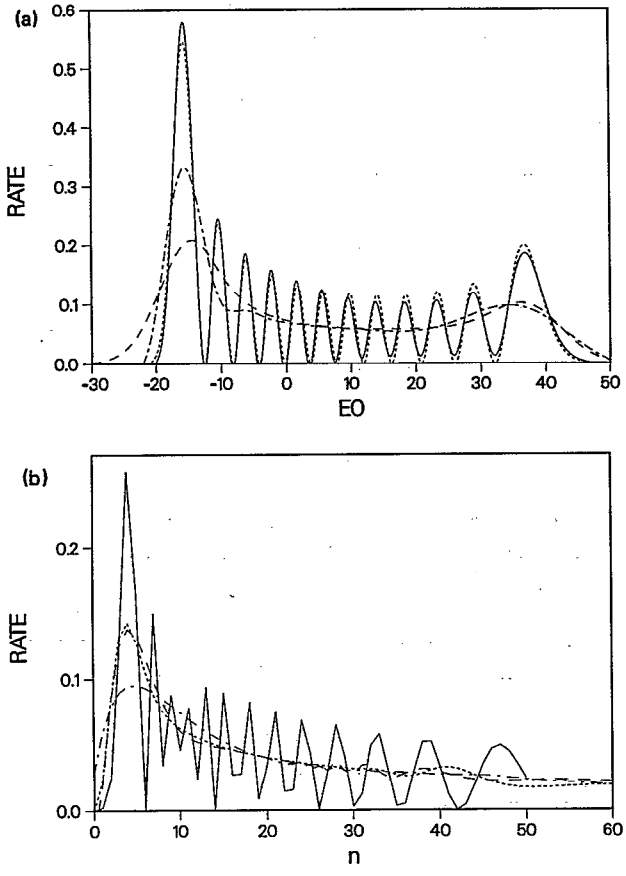

FIG. 2. (a) The transition rate from the $n=11$ level of the harmonic oscillator to the continuum associated with a linear potential. Parameters of the potentials are given in the text. Shown are the exact golden rule result (solid line), the "coherent" FGA calculation (dotted line), and the incoherent FGA results with $A=1$ (dashed line) and $A=30$ (dashed dotted line). (b) The transition rate as a function of the quantum number of the initial harmonic level for $E_0=19.37$ ($V_C=3.5$). Shown are exact golden rule results (solid line) and incoherent FGA results. Using $A=1$ (dashed line), $A=30$ (dotted line), and $A=500$ (dashed–dotted line).

$(m\omega)]^{1/2}$, in the incoherent calculation, we try different choices of this width because in practice the oscillator frequency is not known. In what follows, we use the dimensionless quantity $A=[\hbar/(m\omega)]a$, so that the ground state width is $A^{-1/2}=1$. In Fig. 2(a), we plot the results of the incoherent calculation for two different values of A,$A=1$ and $A=30$. It is obvious that this calculation cannot reproduce the oscillations observed in the exact and in the "coherent" FGA calculations. However, it does reproduce the general trends, e.g., the two peaks at $E_0\sim -15$ and 40 which result from the fact that in the microcanonical distribution, larger weight is associated with phase points near the classical turning points. We also conclude that the choice of the width does not affect the results dramatically. Change of the width by nearly two orders of magnitude does not change the rate by more than a factor of 2 in most of the spectrum.

The exact and incoherent FGA results are shown as functions of the initial energy level in Fig. 2(b). Here $E_0=19.37$ ($V_c=3.5$). As before, the oscillations observed in the exact result are smoothed out in the incoherent FGA

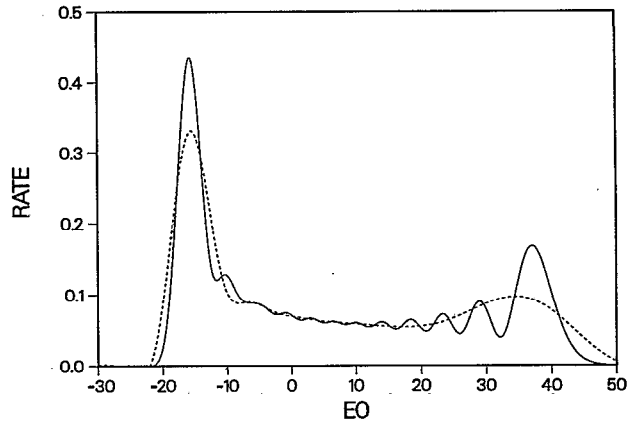

FIG. 3. The transition rate out of the $n=11$ level of the harmonic oscillator. The exact results [from the solid line of Fig. 2(a)] are averaged over intervals of $\Delta E_0=4$ (solid line). Also shown are the incoherent FGA results with $A=30$ from Fig. 2(a) (dotted line).

results, however, the general behavior is again reproduced correctly and as long as not too extreme values of the Gaussian width are chosen, the results do not depend strongly on this width. The latter observation holds particularly for the higher energy states.

Figure 3 compares the incoherent FGA result with $A=30$ to the exact result, the solid line of Fig. 2(a) coarse grained by averaging over E_0 windows of width $\Delta E_0=4$. It is seen that at this resolution, the results agree fairly well. For condensed phase systems where many quantum levels contribute to the initial energy state within the experimental resolution, the incoherent FGA is thus expected to provide a fairly good approximation to the microcanonical rate.

The results obtained for individual levels can be further averaged to get the thermal rate. The temperature T will be expressed in units of $(\hbar\omega)/k_B$. Since the thermal rate is an average of rates from individual quantum levels, we expect that the oscillations associated with the structure of individual wave functions will cancel out, and that the incoherent FGA will perform well even for the simple one dimensional example considered here. Indeed, as shown in Table I, the thermal rate is reproduced correctly by the FGA calculation at high enough temperatures. In the cal-

TABLE I. The exact and FGA (incoherent) thermal rates for two cases in which the same linear and harmonic surfaces (parameters given in the text) are displaced differently, as expressed by the crossing energy V_c. The FGA calculation was performed with $A=6T$.

T	Exact $V_C=3.5$	FGA $V_C=3.5$	Exact $V_C=15$	FGA $V_C=15$
0.5	1.04×10^{-3}	3.95×10^{-4}	4.24×10^{-13}	4.15×10^{-12}
1	1.02×10^{-2}	9.81×10^{-3}	9.64×10^{-8}	-1.4×10^{-8}
2	3.64×10^{-2}	3.70×10^{-2}	8.98×10^{-5}	7.10×10^{-5}
3	5.25×10^{-2}	5.31×10^{-2}	8.63×10^{-4}	8.23×10^{-4}
5	6.45×10^{-2}	6.48×10^{-2}	4.88×10^{-3}	4.87×10^{-3}
10	6.45×10^{-2}	6.47×10^{-2}	1.53×10^{-2}	1.55×10^{-2}
12	6.30×10^{-2}	6.26×10^{-2}	1.78×10^{-2}	1.81×10^{-2}
15	5.87×10^{-2}	5.94×10^{-2}	2.02×10^{-2}	2.08×10^{-2}

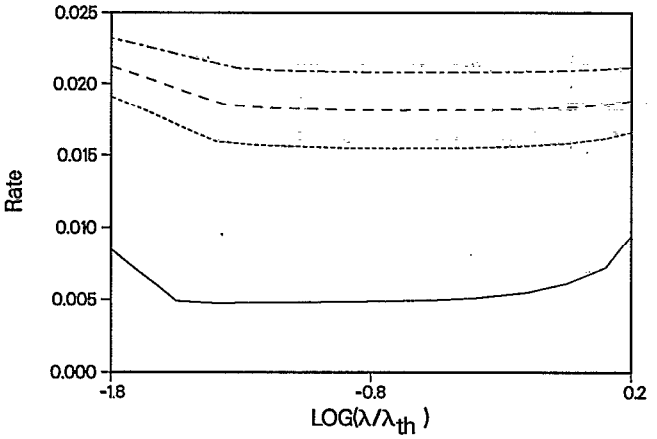

FIG. 4. The thermal FGA rate as a function of the frozen Gaussians width ($\lambda=a^{-1/2}$) for different temperatures $T=5$ (solid line), $T=10$ (dotted line), $T=12$ (dashed line), and $T=15$ (dashed–dotted line). The harmonic and linear surfaces cross at $V_C=15$.

culation summarized in Table I, the width of the Gaussian packets is taken as in Eq. (11), i.e., $A=6T$. However, the result is not strongly sensitive to this choice. In Fig. 4, we plot the dependence of the rate on the chosen Gaussian width. It is seen that for width within two orders of magnitude of the thermal de Broglie wavelength, the results are not sensitive to this width. This results from the fact that the decay of the correlation function is caused, for high T, mainly by cancellation of phases which are independent of the width. This issue is further discussed in Sec. V. It should be noted that if we expand the initial state in a complete basis set of coherent (Gaussians) states, then perform thermal averaging over the initial state distribution, the quality of the resulting rates depends only on the frozen Gaussian approximation, and when the latter is avoided, the rate is exact (within the golden rule), independent of the chosen Gaussian width. This independence is maintained in a large range of this width also in our approximate incoherent sampling, however, the rate does become unphysically dependent on the width when the latter takes extremely large or small values.

For $T\leqslant 1$, the calculation fails as seen in Table I. In this temperature range, the result is also very sensitive to the Gaussian width.

Next we apply to the same model the method recently proposed by Tully for molecular dynamics with electronic transitions (MDET). For completeness, the algorithm is described in Appendix B. One obvious limitation of this method is that electronic transitions are not allowed if the initial energy is below the crossing energy of the two surfaces. Thus, tunneling is essentially forbidden. Another problem in applying this method for the present model is that in contrast to the assertion made in Ref. 5, the average number of trajectories on each potential surface is not necessarily equal to the average of the corresponding diagonal elements of the density matrix. This results from the fact that, when the initial energy is not much higher than the crossing energy, many transitions will be rejected for failing to satisfy the energy conservation criterion, leading to a

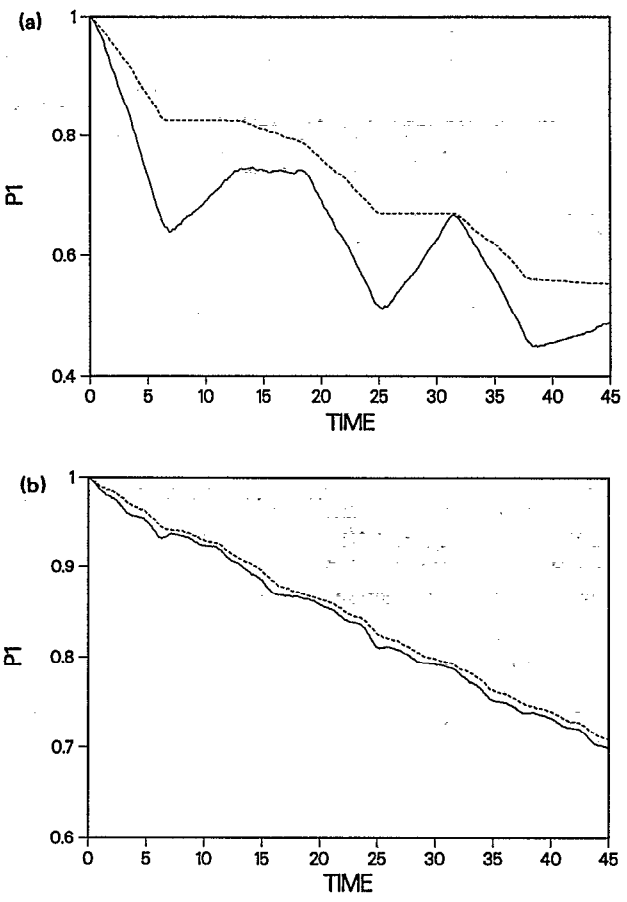

FIG. 5. (a) The average number of trajectories on the harmonic surface [state 1 (dotted line)] and the average of the density matrix element $\rho_{1,1}$ starting at the $n=16$ level of the oscillator. The harmonic and linear surfaces cross at $V_C=15$. (b) The same as (a) starting from the $n=30$ level of the oscillator.

bias in the populations of the electronic states which is not reflected in the value of the diagonal elements of ρ. This is demonstrated in Fig. 5(a).

The potential advantage of the MDET method is that it provides the full temporal evolution of the system and not just the transition rate. Obviously this is also a drawback if the rate is well defined, but small, since very long trajectories may be required.

Figure 5 displays results obtained using this method for the model of coupled harmonic and linear potential surfaces. The simulations were performed with $\alpha=6$, $E_0=47.86$ ($V_c=15$), and $V_{12}=0.5$. Shown are the depletion rates out of two initial eigenstates of the harmonic surface $n=16$ and $n=30$. The initial conditions were sampled from a classical microcanonical distribution with the energy of the initial level. At each initial point, a total of 500 trajectories were generated in order to achieve a convergent result from that point and one hundred such points were used for each initial quantum level. This is a much larger computational effort than that needed to evaluate the golden rule rate.

For the sake of comparison, we have also obtained "exact" numerical results for the same process using a direct solution of the time dependent Schrödinger equation

based on the fast Fourier transform (FFT) algorithm with second-order differencing evaluation of the time derivatives.[27] The FFT simulation was carried out on a grid of 256 points with spacing $\Delta x=0.125$ and with the minimum of the harmonic surface located at position 160 on the grid. In order to perform simulations for long periods of time with this limited grid size, we have followed the procedure used by Heather and Metiu.[28] The wave function propagating on the linear surface is absorbed as it approaches the end of the grid, by multiplying it by the function $f(x)$,

$$f(x)=\{1+\exp[-c(x-\bar{x})]\}^{-1} \tag{16}$$

with $c=12.0$ and $\bar{x}=-18.0$, whenever its value at the grid surface exceeds 10^{-5}.

Figure 5(a) shows $P_1(t)$, the average fraction of trajectories remaining on the harmonic surface at time t, and the average of $\rho_{1,1}(t)$ [Eq. (B3a)] starting from the $n=16$ level of the harmonic potential. It is seen that $\rho_{1,1}(t)$ has a staircase structure which follows P_1 only in a coarse grained sense. When the initial energy is much higher than V_c, transitions are less restricted by the energy conservation criterion, and $\rho_{1,1}$ and P_1 almost coincide as seen in Fig. 5(b), which shows the evolution out of the initial level $n=30$.

A comparison between the exact evolution and the MDET results for the transitions out of the $n=16$ and $n=30$ levels is shown in Fig. 6, which again shows $P_1(t)$ as a function of time as obtained from the MDET algorithm and from exact FFT time evolution. We see that the MDET algorithm underestimates the rate out of the $n=16$ level, whereas it overestimates it for the $n=30$ level. Moreover, while the exact dynamics, for all the initial levels studied, shows an exponential decay of the population in the initial electronic state, the MDET decay is qualitatively different and is in general nonexponential. In spite of this, we have fitted both exact and MDET decay curves to exponentials in order to obtain a measure for the transition rate. The results are shown in Table II together with the golden rule rates obtained from both the exact calculation and from the FGA calculation with $A=30$. Table II shows that (a) the golden rule is a very good approximation for this choice of parameters; (b) unlike the FGA rate which averages the oscillations in the dependence of the exact rate on the initial vibrational level, the MDET shows such oscillations, however, it cannot reproduce their correct positions as functions of the initial energy.

To calculate the thermal rate by the MDET approach, initial conditions are sampled from a Boltzmann distribution on the harmonic surface. Since the evolution is not exponential, and populations in levels lower than the crossing energy do not decay in this approximation, we have characterized the process in terms of $\bar{P}_1(t)=P_1(t)-P_\infty$, where $P_\infty=P_1(t\to\infty)$. $\bar{P}_1(t)$ is fitted to a two exponential evolution

$$\bar{P}_1(t)=\Delta_1 e^{-k_1 t}+\Delta_2 e^{-k_2 t}. \tag{17}$$

This leads to the results shown in Table III for $T=5$, 10, and 15 for potentials crossing at $V_C=15$. Also shown is the initial rate

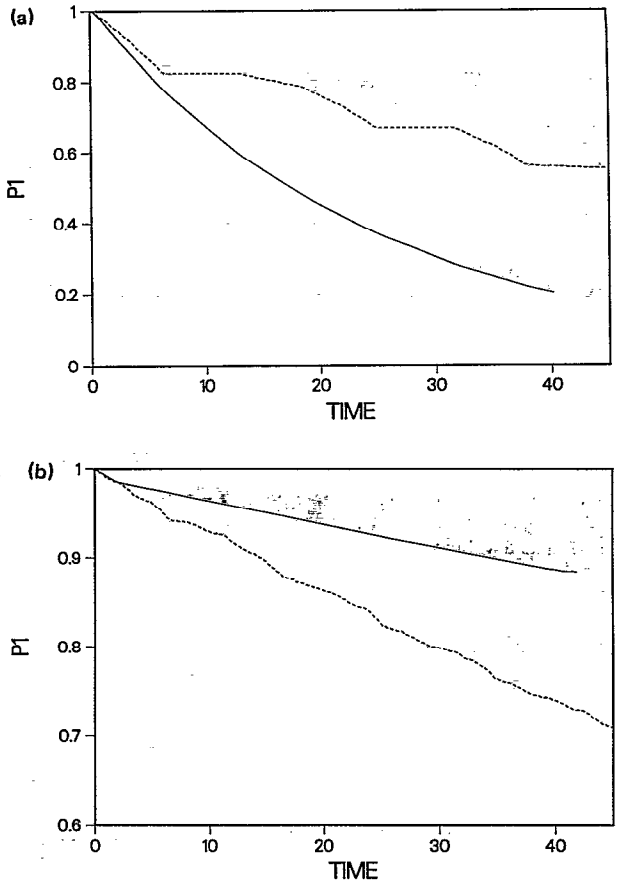

FIG. 6. (a) The comparison between the exact FFT result (solid line) and the MDET result (dotted line) starting with the $n=16$ level of the harmonic surface. (b) The same as (a), starting from the $n=30$ level.

$$k_{\mathrm{MDET}}=-\frac{d}{dt}\ln[P_1(t)]\,|_{t=0}=\Delta_1 k_1+\Delta_2 k_2, \tag{18}$$

which we take as an estimate of the thermal rate. Table III also shows the exact golden rule result from Table I. We see that k_{MDET} underestimates the golden rule rate (which was seen to be practically exact for this choice of parameters) by a factor of ~ 2.

Finally, we consider the adiabatic case in which the value of the coupling constant V_{12} is large. In this case, the

TABLE II. A comparison between the exact FFT, the MDET, the exact golden rule (G.R.), and the FGA (incoherent) transition rates from an initial quantum level of the harmonic surface to the continuum of levels of a linear potential. Parameters of the potentials are given in the text. The crossing energy is $V_C=15$.

n	FFT	MDET	G.R.	FGA
15	3.14	1.65	2.88	1.80
16	3.98	1.44	4.34	1.95
18	0.39	1.49	0.24	1.95
19	1.03	3.43	1.14	1.82
20	2.30	1.40	2.54	1.66
23	1.18	4.17	1.25	1.15
25	1.69	3.51	1.68	0.93
28	0.16	0.72	0.12	0.79
30	0.31	0.78	0.33	0.77

TABLE III. Parameters obtained from the fit of the survival probability $P_1(t)$ on the initial surface, obtained from an MDET calculation, to the function $\Delta_1 e^{-k_1 t}+\Delta_2 e^{-k_2 t}+P_\infty$. Initial conditions are sampled from a classical canonical distribution characterized by a temperature T. The harmonic and linear surfaces cross at $V_C=15$.

T	Δ_1	Δ_2	k_1	k_2	P_∞	k_{MDET}	$k_{\text{exact G.R.}}$
5	0.0325	0.0186	1.15×10^{-2}	0.127	0.951	2.7×10^{-3}	4.88×10^{-3}
10	0.185	0.067	1.28×10^{-2}	0.105	0.756	9.4×10^{-3}	1.53×10^{-2}
15	0.302	0.107	1.49×10^{-2}	0.090	0.604	1.41×10^{-2}	2.02×10^{-2}

golden rule approximation is expected to break down. Indeed for $V_{12}\geqslant 2$, the exact time evolution is nonexponential, with an overall decay much slower than that predicted by the golden rule expression. The MDET method, on the other hand, performs quite well at least at early times. This is seen in Fig. 7, where the probability P_1 to stay on the harmonic surface starting from the $n=23$ level is displayed for three different values of the coupling V_{12}. One feature of the exact dynamics which is not reproduced by the MDET method is the long time behavior of P_1, in particular, for larger values of V_{12}. The observed long time tail results from the fact that part of the wave function remains trapped on the upper *adiabatic* surface. This trapping is not reproduced by the MDET algorithm because of the energy conservation criterion, which does not allow trajectories to reach the upper adiabatic surface. The bottom energy of this surface is V_C+V_{12}, so for $V_C=15$ and $V_{12}>7$, this minimum is above the initial energy $E_{n=23}$. This is not a failure of the algorithm itself, but simply a manifestation of the fact that for large V_{12}, the diabatic energy is not a good measure of the real energy that should be conserved. This observation suggests that in the strongly adiabatic limit, the MDET algorithm will perform better using the adiabatic, rather than the diabatic representation. The initial harmonic state will be represented by a linear combinations of states defined on the two adiabatic surfaces, and the splitting of populations will follow naturally.

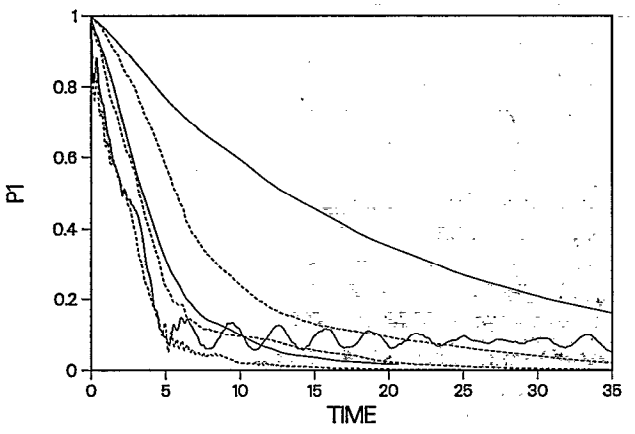

FIG. 7. The exact (solid lines) and MDET (dotted lines) probabilities to remain on the initial harmonic surface starting at the initial $n=23$ harmonic level. Lines showing increasing initial rates correspond to $V_{12}=2$, 4, and 6, respectively.

IV. DISPLACED HARMONIC OSCILLATORS

The displaced harmonic potentials model is commonly used to describe chemical reactions, electron transfer, and other radiationless transitions in molecules and condensed phases. We shall use the simplest version of this model with two mutually displaced identical multidimensional harmonic surfaces

$$V_1=\frac{1}{2}\sum_{j=1}^{N} m_j\omega_j^2 x_j^2, \tag{19}$$

$$V_2=\frac{1}{2}\sum_{j=1}^{N} m_j\omega_j^2(x_j+d_j)^2-\Delta E. \tag{20}$$

In dimensionless units $X_j=(m_j\omega_j/\hbar)^{1/2}x_j$ and $\Delta_j=(m_j\omega_j/\hbar)^{1/2}d_j$, these surfaces become

$$V_1=\frac{1}{2}\sum_{j=1}^{N}\hbar\omega_j X_j^2, \tag{21}$$

$$V_2=\frac{1}{2}\sum_{j=1}^{N}\hbar\omega_j(X_j+\Delta_j)^2-\Delta E. \tag{22}$$

The crossing of these surfaces defines an $N-1$ dimensional surface. The minimal crossing energy U_C obtained by minimizing V_1 subject to the constraint $V_1(\mathbf{X})=V_2(\mathbf{X})$ is

$$U_C=\frac{1}{4E_M}(\Delta E-E_M)^2, \tag{23}$$

where E_M is one-half of the Stokes shift given by

$$E_M=\frac{1}{2}\sum_{j=1}^{N}\hbar\omega_j\Delta_j^2. \tag{24}$$

The golden rule expression for the thermal rate in this model can be evaluated analytically.[29] The canonically averaged correlation function $C(t)$ [Eq. (13)] is given by

$$C(t)=\frac{V^2}{\hbar^2}\exp\{G_+(t)+G_-(t)-G-i\Delta Et/\hbar\}, \tag{25}$$

where

$$G_+(t)=\frac{1}{2}\sum_{j=1}^{N}\Delta_j^2(\bar{n}_j+1)e^{i\omega_j t}, \tag{26a}$$

$$G_-(t)=\frac{1}{2}\sum_{j=1}^{N}\Delta_j^2\bar{n}_j e^{-i\omega_j t}, \tag{26b}$$

$$G=G_+(0)+G_-(0)=\sum_{j=1}^{N}\Delta_j^2(\bar{n}_j+1/2), \tag{26c}$$

$$\bar{n}_j+1/2=\frac{1}{2}\coth\left(\frac{\hbar\omega_j}{2k_BT}\right). \tag{26d}$$

G is referred to as the coupling strength. A convenient representation is

$$G=\frac{E_M}{\hbar\langle\omega\rangle}\coth\left(\frac{\hbar\langle\omega\rangle}{2k_BT}\right), \tag{27}$$

where $\langle\omega\rangle$ is the characteristic, e.g., averaged frequency. The case $G\gg 1$ which is obtained for $k_BT\gg\hbar\langle\omega\rangle$ and/or large Δ_j is referred to as the strong coupling limit. In addition, increasing the number of shifted oscillators, i.e., nuclear modes which are strongly coupled to the electronic transitions, also takes the system towards this limit. In the strong coupling limit, the correlation function decays fast and on the relevant time scale $G_+(t)$ and $G_-(t)$ can be expanded in a power series of t to second order

$$G_+(t)+G_-(t)\cong G+\frac{it}{2}\sum_{j=1}^{N}\omega_j\Delta_j^2-\frac{1}{2}D^2t^2, \tag{28a}$$

$$D^2\equiv\sum_{j=1}^{N}\omega_j^2\Delta_j^2(\bar{n}_j+1/2). \tag{28b}$$

Using this approximation (6) leads to

$$k_{1\to 2}=\frac{V^2}{\hbar D}\sqrt{2\pi}\exp\left(\frac{-2E_M}{\hbar^2D^2}U_C\right). \tag{29}$$

For $k_BT\gg\hbar\omega$, this becomes

$$k_{1\to 2}=\frac{V^2}{\hbar}\left(\frac{\pi}{k_BTE_M}\right)^{1/2}e^{-U_C/k_BT}, \tag{30}$$

whereas for low temperature, we get

$$k_{1\to 2}=\frac{V^2}{\hbar}\left(\frac{\pi}{\langle\omega\rangle E_M}\right)^{1/2}\exp\left[-\frac{U_C}{(1/2)\hbar\langle\omega\rangle}\right]. \tag{31}$$

The FGA result for this case can also be obtained analytically since it involves only Gaussian integrals. The result for $J(t)$ [Eq. (8b)] is

$$J(t)=\exp\left\{-\sum_{j=1}^{N}\left[\frac{A_j}{4}\Delta_j^2(1-\cos\omega_jt)^2+\frac{\Delta_j^2}{4A_j}\sin^2\omega_jt-\frac{i}{2}\Delta_j^2\sin(\omega_jt)-i\Delta_jX_j\sin(\omega_jt)-i\Delta_jP_j(1-\cos\omega_jt)\right]\right\}, \tag{32}$$

$\{X_j\}$ and $\{P_j\}$, $j=1,\ldots N$ are the center positions and momenta of the frozen Gaussians and $A_j=[\hbar/(m_j\omega_j)]a_j$. A classical averaging over the thermal distribution of $\{X_j\}$ and $\{P_j\}$ leads to

$$C(t)=\frac{V^2}{\hbar^2}\langle J(t)\rangle_T$$
$$=\frac{V^2}{\hbar^2}\exp\left[-i\Delta Et/\hbar+\frac{i}{2}\sum_{j=1}^{N}\Delta_j^2\sin(\omega_jt)-\sum_{j=1}^{N}\frac{k_BT}{\hbar\omega_j}\Delta_j^2(1-\cos\omega_jt)+\frac{A_j}{4}\Delta_j^2(1-\cos\omega_jt)^2+\frac{\Delta_j^2}{4A_j}\sin^2\omega_jt\right]. \tag{33}$$

In the strong coupling limit, an expansion of the exponent in powers of t up to second order is valid. The requirement that the short time expansions of the exponents in the exact and the FGA results [Eqs. (26) and (33), respectively] are identical leads to

$$\sum_{j=1}^{N}\left(\frac{k_BT}{\hbar\omega_j}\Delta_j^2+\frac{\Delta_j^2}{2A_j}\right)\omega_j^2=D^2, \tag{34}$$

or

$$A_j=\left[\coth\left(\frac{\hbar\omega_j}{2k_BT}\right)-\frac{2k_BT}{\hbar\omega_j}\right]^{-1}; \tag{35}$$

for high temperatures $\hbar\omega_j/k_BT<1$, this becomes

$$a_j=\frac{m_j\omega_j}{\hbar}A_j=\frac{6m_jk_BT}{\hbar^2} \tag{36}$$

as in Eq. (11). The error in this estimate of the width is already less then 10% at a temperature for which $\hbar\omega_j/k_BT=0.5$. At low temperatures, a_j approaches the width of the ground state according to

$$a_j=\frac{m_j\omega_j}{\hbar}+\frac{2m_jk_BT}{\hbar^2}. \tag{37}$$

The high temperature result (36) is useful for realistic simulations since all the quantities are known and we can immediately assign a width to each particle. The low temperature result is less useful unless we use a local normal mode representation so that a frequency is assigned for each degree of freedom. Alternatively, as seen below, it is possible to estimate the average frequency and use it in Eq. (37).

At $T=0$, the FGA results are exact, provided that we take $a_j=m_j\omega_j/\hbar$. This follows from the fact that the ground state wave function is a Gaussian of such width centered at $X_j=P_j=0$. The FGA propagation of this wave function on a harmonic surface of frequency ω_j is exact.

A comparison between the "exact" golden rule and the FGA results is shown for a system of 20 displaced harmonic oscillators in Fig. 8. The oscillators are characterized by equal displacements $\Delta=\sqrt{5}$, which corresponds to the strong coupling limit $G=50$ at $T=0$. Two sets of frequencies are studied. The frequencies of set A are, in arbitrary units, distributed uniformly between 0.7 and 1.3, with average frequency $\langle\omega\rangle=0.962$ and $\Delta E=80$. This corresponds to $U_C=5.29$. The frequencies of set B are also equally spaced in the range between 2 and 4, with average frequency 2.873, $\Delta E=239$, and $U_C=15.8$. Figure 8 shows

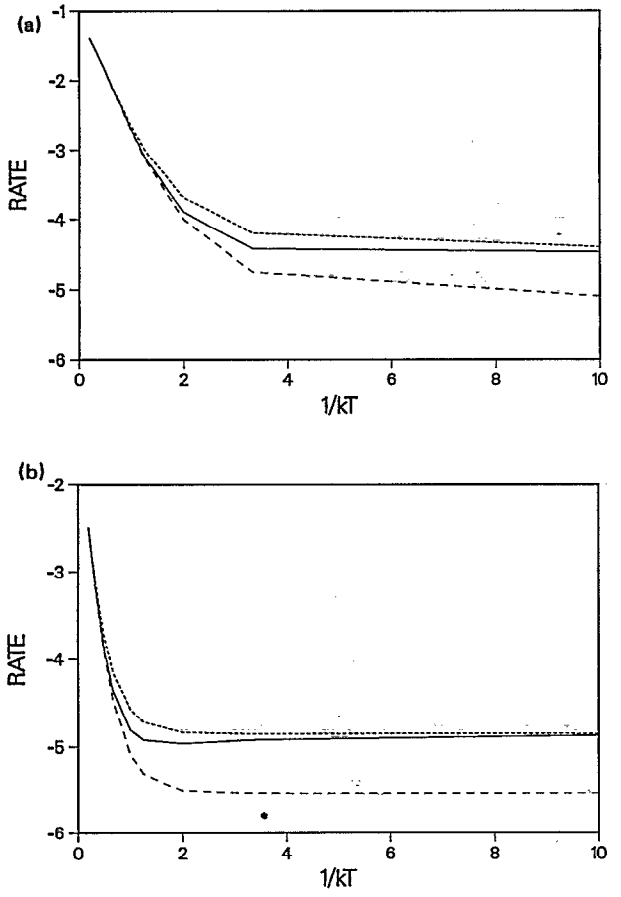

FIG. 8. The transition rate between the displaced harmonic surfaces as function of the temperature. (a) Parameters from set A (see the text). (Solid line) exact golden rule; (dotted line) FGA with width given by Eq. (35); (dashed line) the strong coupling limit [Eq. (29)]. (b) The same as (a) using the parameters from set B.

the exact golden rule rate, the semiclassical rate with the width given by Eq. (35), and the strong Coupling limit [Eq. (29)]. It is seen that the FGA provides a good approximation to the exact rate in the entire temperature range. In both extreme limits $T\to\infty$ and $T\to 0$, the FGA result becomes exact.

The sensitivity of the result to the chosen Gaussian width can be inferred from the results of Tables IV and V which give the rate for several temperatures with different widths. At low temperatures $k_BT<\hbar\langle\omega\rangle$, the result is very sensitive to the width. The reason is that at such temperatures the decay of the correlation function is caused

TABLE IV. A comparison between the exact thermal rate and the FGA thermal rate for the transition between displaced harmonic surfaces characterized by the parameters of set A (see the text). The FGA is calculated using the width parameter A_j of Eq. (35) multiplied by a constant factor γ.

T	$\gamma=0.1$	$\gamma=1$	$\gamma=5$	Exact
0.1	4.42×10^{-2}	3.36×10^{-5}	-8.71×10^{-6}	3.92×10^{-5}
1	1.06×10^{-2}	1.94×10^{-3}	3.18×10^{-4}	2.17×10^{-3}
2	1.85×10^{-2}	1.36×10^{-2}	1.35×10^{-2}	1.34×10^{-2}
5	4.04×10^{-2}	3.99×10^{-2}	4.04×10^{-2}	3.97×10^{-2}

TABLE V. The same as Table IV, with the parameters characterizing the harmonic surfaces taken from set B (see the text).

T	$\gamma=0.1$	$\gamma=1$	$\gamma=5$	Exact
0.1	1.27×10^{-2}	1.32×10^{-5}	3.86×10^{-6}	1.37×10^{-5}
1	6.63×10^{-3}	1.54×10^{-5}	2.55×10^{-5}	2.66×10^{-5}
2	3.84×10^{-3}	1.34×10^{-4}	-2.20×10^{-4}	1.84×10^{-4}
5	5.15×10^{-3}	3.09×10^{-3}	2.86×10^{-3}	3.12×10^{-3}

mainly by the terms in the exponent of $C(t)$ [Eq. (33)], which contain the width explicitly. At higher temperature, these terms become increasingly less important, and in the high temperature limit, the result is nearly insensitive of the width, within reasonable bounds about the thermal de Broglie length. The choice (36) is optimal as discussed above. The sensitivity of the low temperature result to the chosen width of the Gaussian wave packets and the uncertainty in choosing the width, unless a normal mode representation for the nuclear degrees of freedom is known, make the low temperature calculation more complicated. It is possible to choose the Gaussian width as an average over the distribution of molecular frequencies (this can be obtained from a Fourier analysis of the classical motion) in order to obtain an order of magnitude estimate (see Table VI). Alternatively, in many applications, nuclear modes may be separated into two groups—one containing high frequency "inner sphere" modes that can be described as harmonic oscillators and the other group of low frequency "outer sphere" modes for which the high temperature limit may be valid. Such systems may be studied by using the high temperature limit and the harmonic approximation separately for the different groups of the modes.

V. DYNAMICS OF ELECTRON HYDRATION

The formation and relaxation of solvated electrons have been the focus of intensive research for a long time.[30] It is only recently, however, that the primary step in this complex process has become accessible to experimental observation. Recent experimental results[18,19] suggest that the solvation dynamics following electron ejection into liquid water involve at least one, and possibly more intermediates. In particular, a relaxation process from a transient species that absorbs in the near IR to the fully solvated electron was reported with relaxation time reported to be $\sim$240 fs by Migus *et al.*[18] and 540±50 fs by Long *et al.*[19] These experimental results cannot be explained by either dielectric theories or adiabatic simulations, which, in contrast to experimental observation, predict continuous shift

TABLE VI. A comparison between the exact golden rule rate and the FGA rate at $T=0$. The width is taken from Eq. (37) with equal frequency (either $\langle\omega\rangle$ or $\langle\omega^2\rangle/\langle\omega\rangle$) for all the oscillators.

Set	$\langle\omega\rangle$	$\langle\omega^2\rangle/\langle\omega\rangle$	Exact
A	5.62×10^{-5}	4.92×10^{-5}	3.92×10^{-5}
B	2.14×10^{-5}	1.72×10^{-5}	1.38×10^{-5}
$A+B$	6.87×10^{-4}	2.39×10^{-4}	1.12×10^{-4}

of the absorption peak. Assuming that the intermediate state is an excited state of the hydrated electron, this relaxation process may be explained by a nonadiabatic transition from this excited state to the ground state. Reasonable choices of such excited states are the three nearly degenerate p like states which carry most of the oscillator strength of the 1.7 eV absorption of the fully hydrated electron.[22(a),23–25] This section describes the calculation of the rate of this process using the procedure described in Sec. II. A preliminary report of this calculation was published.[17]

The calculation is based on a mixed quantum-classical adiabatic simulation[22] in which the electron is described quantum mechanically and the water molecules classically. The electron is restricted to remain in a single adiabatic state (either an excited or the ground state) at the instantaneous water configuration by a combination of imaginary time propagation and orthogonalization to lower state(s).[22] The waters move classically under their mutual interactions and the expectation value of the water–electron interaction. We use the RWK2-M (flexible) water potential[31] and the electron–water pseudopotential developed by Barnett *et al.*[32] The simulations are performed on a cluster of 128 water molecules and one excess electron. Simulation of the absorption spectrum of this system indicates that it represents quite well the electron in bulk water.[22(a)]

As discussed in Sec. II, the information needed to calculate the golden rule rate can be obtained from the adiabatic trajectories. All relevant electronic states and states and energies are evaluated at each nuclear configuration. First, a long equilibrium trajectory (at temperature 300 K) is obtained in this way. From this trajectory, configurations are selected at 75 fs intervals for the rate calculation. Each of these configurations is the starting point for the calculation of the correlation function $C(t)$ of Eq. (8). In the latter calculation, two trajectories are calculated, both starting from that same initial conditions. In one, the nuclei move in the potential of the electron in its initial (excited) state. This trajectory is in fact part of the equilibrium trajectory obtained earlier. In the second trajectory, the nuclei are subjected to the final (ground) state potential. The overlap (as a function of time) between the *nuclear wave functions*—the frozen Gaussians associated with the classical nuclear positions and momenta, along these two trajectories, together with the adiabatic electronic energies and the nuclear positions and momenta associated with the initial electronic state—are the needed input for calculating $C(t)$ of Eq. (8).

An important technical point concerns the nondiagonal terms ($l \neq l'$) in Eq. (8). For symmetry reasons, these terms should cancel out in a proper averaging, but in our limited statistics, their inclusion increases the statistical error. We have therefore disregarded these terms at the outset, replacing Eq. (8) by

$$C(t)=\left\langle \sum_l \mathbf{F}_l^*\mathbf{R}^{(1)}(t)\cdot\mathbf{v}_l^{(1)}(t)\mathbf{F}_l\mathbf{R}^{(1)}(0)\cdot\mathbf{v}_l^{(1)}(0)J(t)\right\rangle_T . \tag{38}$$

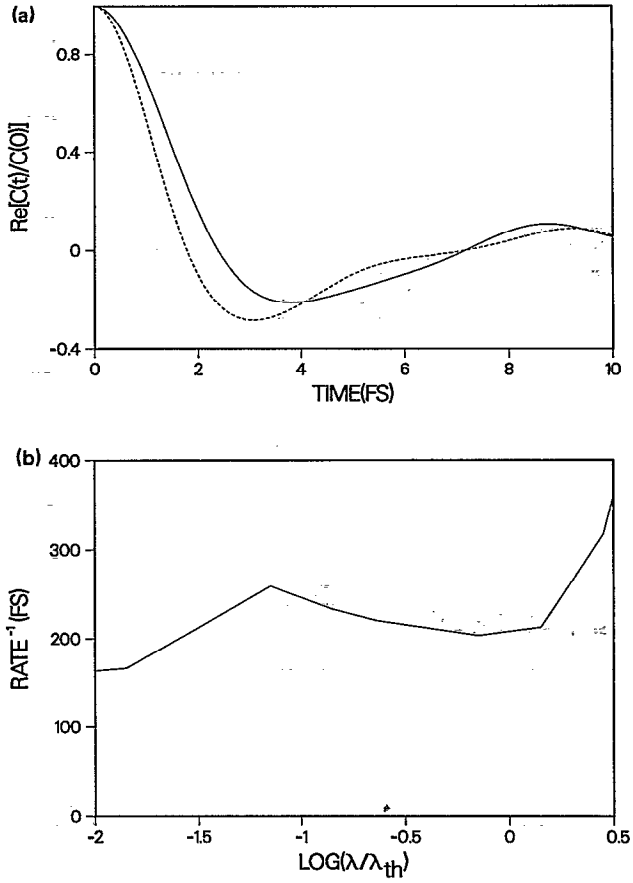

FIG. 9. (a) The correlation function $C(t)$ for H_2O (solid line) and D_2O (dotted line). (b) The nonadiabatic rate for the transition from the first excited state to the ground state of the electron in H_2O as a function of $\log_{10}(\lambda/\lambda_{th})$. $\lambda=a^{-1/2}$.

Fifteen trajectories of 10 fs each were used to calculate an approximate thermal average. This is obviously poor statistics dictated by our limited computing resources, but should be enough for crude estimates. Note that in our earlier report,[17] we have imposed the Condon approximation, replacing Eq. (38) by $C(t)=\Sigma_l\langle[\mathbf{F}_l(0)\cdot\mathbf{v}_l(0)]^2\rangle_T\langle J(t)\rangle_T$. The results reported below are based on the full correlation function (38). We have also corrected a mistake in our previous calculation,[17] which changed the results for the rate by a factor of 2.

Figure 9(a) shows the correlation function $C(t)$ as a function of time for electrons in H_2O and D_2O. The Gaussian width in this calculation is that of Eq. (11). The correlation function decays on a time scale of 10 fs which provides *a posteriori* justification for the use of frozen Gaussians in this calculation. The calculated rates are shown, as functions of the width of the frozen Gaussians, in Fig. 9(b). Using the value for the width from Eq. (11), the transition time in the regular water environment is found to be $k^{-1}\cong 220$ fs. The same procedure gives $k^{-1}\cong 800$ fs for D_2O [we also observe for D_2O a stronger dependence of the calculated rate on the chosen width, however, this may be an artifact of the statistical error (see below)]. We find $k^{-1}\cong 800$ fs. The result for H_2O is very close to the experimental values cited above. However, the isotope

effect is much larger than found experimentally (35% by Long *et al.*,[33] in an experiment that could be affected by the isotope effect in the electron–parent ion recombination process,[34] and a very small effect of ~10% by Gauduel *et al.*[35]). As already observed in the previous sections, the rate is not very sensitive to the Gaussian width, which in Fig. 9(b) spans a scale of two orders of magnitude, as long as not too extreme values are used. This is in agreement with the results of the previous sections.

It is encouraging that the results obtained in this calculation are of the same order of magnitude as the experimentally observed rates. The disagreement between the observed isotope effect and between the calculated one, however, raises doubts about this suggested interpretation of the intermediate process in electron hydration. It should be emphasized that the present calculation is not intended to give more than an order of magnitude estimate of the rate because of the very small number of trajectories used. It suffers from a few other drawbacks: (a) the electron–water pseudopotential used in the simulation was obtained by fitting with quantum chemistry calculations in the ground state,[32] but is used here to run trajectories on the excited state. (b) The use of classical distributions for the thermal averaging is a source of error, especially for the high frequency modes. (c) Only one of the three closely lying *p*-like excited states of the hydrated electron is used in the present calculation. (d) The fact that the rate is obtained from an integral over the correlation function $C(t)$ which in the present calculation contains large positive and negative parts [see Fig. 9(a)] is another source of numerical error. This error can be made smaller by computing more trajectories. Within the *physical* approximations made here, this is probably the most important source of *numerical* error in the present calculation. We do not believe, however, that the calculated isotope effect is an artifact of these simplifications because, on physical grounds, we expect that nuclear motions involving hydrogens are the main accepting modes in this relaxation process, as in other radiationless transitions in molecular systems.[29]

VI. CONCLUSIONS

The computation of nonadiabatic transition rates for condensed phase processes poses practical and conceptual difficulties. These are related to the inherent quantum nature of the process, which takes place in an otherwise essentially classical environment. In this paper, we have presented and tested a procedure for evaluating such rates using the golden rule approximation and getting the information needed for its semiclassical evaluation from classical trajectories. The numerical approach makes it possible to avoid using simplified models such as harmonic potentials and the Condon approximation, usually invoked in analytical procedures. An important simplifying feature is the fact that, for condensed phase processes, the lifetime of the correlation function related to the golden rule rate is very short, making it possible to use frozen Gaussians imposed on the classical trajectories. Another important aspect of this approach is that it does not rely on the knowledge of the global electronic potential surfaces of the initial and final electronic states, only on their local properties. This makes it possible to evaluate the needed information along the trajectory. Finally, the calculation focuses directly on the rate. When the latter exists, this is a much more economical route for evaluating it then using the full time evolution.

We have tested the method by applying it to simple models which are also amenable to exact calculations—a coupled harmonic-linear potentials model and the displaced harmonic oscillators model. For the first, the method appears to work well, provided that the temperature T is not too low. For the latter, it works well for all T provided that a particular, well-defined procedure for choosing the frozen Gaussian width is taken. For the first model, we have also tested and compared a procedure recently proposed by Tully. Tully's algorithm is valuable because it provides a simple way to calculate an approximation for the full time evolution. However, when a rate exists and the golden rule is valid, our approach is shown to be superior.

We have applied the method for calculating the rate for the nonadiabatic relaxation from the first excited to the fully solvated ground state of the hydrated electron. It is encouraging that the results are at the same order of magnitude as the experimentally observed rate between the intermediate ("wet") and the final ("solvated") forms of the hydrated electron. However, the large predicted isotope effect raises questions concerning this interpretation of the observed process. Nevertheless, this application demonstrates that such calculations can be performed in a very complicated many body systems.

Since the calculation is based on the golden rule expression for the rate, it will fail when the latter does. Furthermore, the classical thermal sampling of the initial distribution and the high temperature approximation inherent in the choice of the frozen Gaussian width in all but harmonic oscillator models introduce new sources of error. These procedures can be improved; e.g., a Wigner distribution could be used for the initial sampling or a local harmonic approximation[36] to the potential surfaces could be used in order to avoid the uncertainty in choosing the Gaussian width.[37] Finally, generalizations of the simple golden rule rates (e.g., the rate for a superexchange model of electron transfer in bridged systems[38]) can be computed in similar ways to those described here. These and other developments of this approach will be described in future publications.

APPENDIX A

Here we outline the calculation of the golden rule rate of transition between the harmonic and the linear potential. We start with the expression for this rate between the nth level of the harmonic potential and the continuum of states on the linear potential

$$W_{n\to\text{cont}}=\frac{2\pi}{\hbar}V^2\int dE\,\rho(E)\,|\langle E|n\rangle|^2\delta(E+E_0-E_n). \tag{A1}$$

$|E\rangle$ is an eigenstate of the Hamiltonian $H=\frac{1}{2}P^2+\alpha X$, corresponding to the eigenenergy E. The wave function of the state E is the Airy function

$$\Psi_E(X)=\langle X|E\rangle=2^{1/3}\alpha^{-1/6}\ \mathrm{Ai}[(2\alpha)^{1/3}(X-E/\alpha)]. \tag{A2}$$

The normalization is chosen such that $\rho(E)=1$. The overlap integral $\langle E|n\rangle$ is obtained by using the following representation of the Airy wave function:[39]

$$\Psi_E(X)=\frac{1}{2\pi\sqrt{\alpha}}\int_{\infty}^{\infty} dk\,\exp[ik^3/6\alpha+ik(X-E/\alpha)], \tag{A3}$$

the overlap integral is

$$\begin{aligned}\langle E|n\rangle&=\int_{\infty}^{\infty} dX\,\Psi_E^*(X)\Psi_n(X)\\&=\int_{-\infty}^{\infty} dX\frac{1}{2\pi\sqrt{\alpha}}\int_{-\infty}^{\infty} dk\\&\quad\times\exp[-ik^3/6\alpha-ik(X-E/\alpha)]\Psi_n(X),\end{aligned} \tag{A4}$$

where $\Psi_n(X)$ is the wave function associated with the nth level of the harmonic oscillator. This leads to

$$\langle E|n\rangle=\frac{1}{\sqrt{2\pi\alpha}}\int_{-\infty}^{\infty} dk\,\exp[-ik^3/6\alpha+ikE/\alpha]\tilde{\Psi}_n(k), \tag{A5}$$

where $\tilde{\Psi}_n(k)$, the Fourier transform of $\Psi_n(x)$, is given by

$$\tilde{\Psi}_n(k)=(-i)^n\Psi_n(x=k). \tag{A6}$$

We are left with the simple integral (A5) over k, which is performed numerically using Filon's method.[39]

APPENDIX B

Here we give a brief description of Tully's MDET algorithm which is tested in Sec. III within the coupled harmonic and linear potentials model.

The electronic wave function is given in the diabatic representation by

$$\begin{aligned}\Psi(t)&=C_1(t)\exp\left[-i\int d\tau\,V_1(\tau)\right]\Phi_1\\&\quad+C_2(t)\exp\left[-i\int d\tau\,V_2(\tau)\right]\Phi_2.\end{aligned} \tag{B1}$$

V_1 and V_2 are the diabatic potential surfaces which depend on time via the time dependence of the nuclear coordinates. ϕ_1 and ϕ_2 are assumed here to be independent of the nuclear coordinates. (This assumption can be relaxed.) The density matrix is defined according to

$$\rho_{ij}=C_iC_j^* \tag{B2}$$

and its equation of motion are

$$\dot{\rho}_{11}=-2V_{12}\,\mathrm{Im}\left(\exp\left[-i\int d\tau[V_1(\tau)-V_2(\tau)]\right]\rho_{12}\right), \tag{B3a}$$

$$\dot{\rho}_{12}=iV_{12}\exp\left[i\int d\tau[V_1(\tau)-V_2(\tau)]\right](\rho_{11}-\rho_{22}) \tag{B3b}$$

and similar equations for $\dot{\rho}_{22}$ and $\dot{\rho}_{21}$. The nuclear motion at each time step takes place on a single potential surface and is determined by the classical equations of motion. The following switching probability per time step is defined for a switch of the nuclear motion from surface i to surface j:

$$P_{\mathrm{switch}}=\frac{\dot{\rho}_{jj}\Delta t}{\rho_{ii}}, \tag{B4}$$

where $\dot{\rho}_{jj}$ is given by Eq. (B3a) or its equivalent with 1 and 2 interchanged, and where Δt is the time step used in the simulation. This switching probability is designed to make the *average* number of trajectories $\langle N_i\rangle$ on the ith surface at time t equal to $\rho_{ii}(t)$ and to achieve this averaging property using the smallest number of state switches. (Note, however, that contrary to the assertion of Ref. 5, this equality between $\langle N_i\rangle$ and ρ_{ii} does not always hold, as discussed in Sec. III.) At each time step, a random number ξ is generated from a uniform distribution between 0 and 1. If $\xi<P_{\mathrm{switch}}$, a switch is made, after which the trajectory is continued on the new surface with momentum modified in order to conserve energy. If energy conservation cannot be satisfied, the switch is denied. The method is easily generalized to the case with more then two potential surfaces and for representations other than diabatic (see Ref. 5 for details).

ACKNOWLEDGMENTS

This research was supported in part by the Basic Research Fund of the Israel Academy of Science. A. N. thanks R. Kosloff, H. Metiu, and M. Ratner for helpful discussions.

[1] (a) See papers in Comp. Phys. Commun. **63**, special issue on "Time Dependent Methods in Quantum Dynamics" (1991); (b) D. Chandler and P. G. Wolynes, J. Chem. Phys. **74**, 4078 (1981); D. Thirumalai and B. J. Berne, Comp. Phys. Commun. **63**, 415 (1991); N. Makri, *ibid.* **63**, 389 (1991); (c) B. J. Berne and D. Thirumalai, Annu. Rev. Phys. Chem. **37**, 401 (1986); (d) M. Parrinello and A. Rahman, J. Chem. Phys. **80**, 860 (1984); U. Landman, D. Scharf, and J. Jortner, Phys. Rev. Lett. **54**, 1860 (1985); (e) R. Car and M. Parrinello, *ibid.* **55**, 2471 (1985); (f) P. A. M. Dirac, Proc. Cambridge Philos. Soc. **26**, 376 (1930); A. D. Mclachlan, Mol. Phys. **7**, 139 (1974); D. Kumamoto and R. Silbey, J. Chem. Phys. **75**, 5164 (1981); R. H. Bisseling, R. Kosloff, R. B. Gerber, M. A. Ratner, L. Gibson, and C. Cerjan, *ibid.* **87**, 2760 (1987); G. Wahnstrom, B. Carmeli, and H. Metiu, *ibid.* **88**, 2478 (1988); (g) Z. Kotler, E. Neria, and A. Nitzan, Comp. Phys. Commun. **63**, 243 (1991).

[2] (a) A. Warshel and W. W. Parson, Annu. Rev. Phys. Chem. **42**, 279 (1991); (b) R. A. Kuwarski, J. S. Bader, D. Chandler, M. Sprik, M. L. Klein, and R. W. Impey, J. Chem. Phys. **89**, 3248 (1989).

[3] N. Makri and W. H. Miller, J. Chem. Phys. **87**, 5781 (1987).

[4] Z. Kotler, A. Nitzan, and R. Kosloff, Chem. Phys. Lett. **153**, 483 (1988).

[5] J. C. Tully, J. Chem. Phys. **93**, 1061 (1990).

[6] J. Campos-Martinez and R. D. Coalson, J. Chem. Phys. **93**, 4740 (1990).

[7] S. Sawada and H. Metiu. J. Chem. Phys. **84**, 227 (1985).

[8] J. C. Tully and R. M. Preston, J. Chem. Phys. **55**, 562 (1971).

[9] L. D. Landau, Phys. Z. Sov. **1**, 88 (1932); **2**, 46 (1932); C. Zener, Proc. R. Soc. London Ser. A **137**, 696 (1932).

[10] (a) F. Webster, J. Schnitker, M. S. Friedrich, R. A. Friesner, and P. J. Rossky, Phys. Rev. Lett. **66**, 3172 (1991); (b) F. Webster, P. J. Rossky, and R. A. Friesner, Comp. Phys. Commun. **63**, 494 (1991).

[11] P. Pechukas, Phys. Rev. **181**, 166 (1974); **181**, 174 (1974).
[12] B. Space and D. F. Coker, J. Chem. Phys. **94**, 1976 (1991); **96**, 652 (1992).
[13] (a) E. J. Heller, J. Chem. Phys. **68**, 2066 (1978); (b) S. Y. Lee and E. J. Heller, *ibid.* **71**, 4777 (1979).
[14] M. F. Herman, J. Chem. Phys. **87**, 4779 (1987); **87**, 4794 (1987).
[15] P. Vilarreal, S. Miret-Artés, O. Roncero, G. Delgado-Bario, J. A. Beswick, N. Halberstadt, and R. D. Coalson, J. Chem. Phys. **94**, 4230 (1991).
[16] K. Haug and H. Metiu, J. Chem. Phys. **97**, 4781 (1992).
[17] E. Neria, A. Nitzan, R. N. Barnett, and U. Landman, Phys. Rev. Lett. **67**, 1011 (1991).
[18] A. Migus, Y. Gauduel, J. L. Martin, and A. Antonetti, Phys. Rev. Lett. **58**, 1559 (1987).
[19] F. H. Long, H. Lu, and K. B. Eisenthal, Phys. Rev. Lett. **64**, 1469 (1990).
[20] E. J. Heller, J. Chem. Phys. **75**, 2923 (1981).
[21] M. J. Davis and E. J. Heller, J. Chem. Phys. **71**, 3383 (1979).
[22] (a) R. N. Barnett, U. Landman, and A. Nitzan, J. Chem. Phys. **89**, 2242 (1989); (b) **93**, 8187 (1990).
[23] R. N. Barnett, U. Landman, G. Rajagopal, and A. Nitzan, Isr. J. Chem. **30**, 85 (1990).
[24] P. J. Rossky and J. Schnitker, J. Phys. Chem. **92**, 4277 (1988).
[25] A. Wallqvist, G. Martyna, and B. J. Berne, J. Phys. Chem. **92**, 1721 (1991).
[26] E. J. Heller, J. Chem. Phys. **64**, 63 (1976).
[27] D. Kosloff and R. Kosloff, J. Comput. Phys. **52**, 35 (1983).
[28] R. Heather and H. Metiu, J. Chem. Phys. **86**, 5009 (1987).
[29] R. Engelman and J. Jortner, Mol. Phys. **18**, 145 (1970).
[30] E. Hart and M. Anbar, *The Hydrated Electron* (Wiley, New York, 1970).
[31] J. R. Riemers, R. O. Watts, and M. L. Klein, Chem. Phys. **64**, 95 (1982); J. R. Riemers and R. O. Watts, *ibid.* **85**, 83 (1984).
[32] R. N. Barnett, U. Landman, C. L. Clevland, and J. Jortner, J. Chem. Phys. **88**, 4421 (1988).
[33] F. H. Long, H. Lu, and K. B. Eisenthal, Chem. Phys. Lett. **160**, 464 (1989).
[34] K. B. Eisenthal (private communication).
[35] Y. Gauduel, S. Pommeret, and A. Antonetti, J. Phys. Chem. **95**, 533 (1991).
[36] B. Hellsing, S. I. Sawada, and H. Metiu, Chem. Phys. Lett. **122**, 303 (1985).
[37] E. Neria and A. Nitzan (to be published).
[38] M. Todd, A. Nitzan, and M. Ratner, J. Phys. Chem. **97**, 29 (1993).
[39] M. Abramowitz and I. R. Stegun, *Handbook of Mathematical Functions* (Dover, New York, 1972).